A facile Shape-Controlled Synthesis of highly photoactive Fluorine containing TiO2 nanosheets with high {001} facet exposure

M.A. Lara[1,2], M.J. Sayagués[1], J.A. Navío[1], M.C. Hidalgo[1]*

[1]*Instituto de Ciencia de Materiales de Sevilla (ICMS), Consejo Superior de Investigaciones Científicas CSIC - Universidad de Sevilla, Américo Vespucio 49, 41092 Sevilla, Spain.*

[2]*Departamento Cristalografía, Mineralogía y Química Agrícola, Universidad de Sevilla, C/Profesor García González s/n, 41012 Sevilla, Spain*

Abstract

Surface fluorinated TiO2 materials with high {001} facet exposure were prepared by a simple and high yield preparation procedure. Faceted/fluorinated samples showed a high photocatalytic performance not only in oxidation processes, tested inphenol and Methyl Orange degradation, but also in a reduction process as Cr(VI) photoreduction. Reaction rates for these materials greatly exceeded the ones obtained for materials prepared without Fluorine addition and for commercial TiO2 Degussa (Evonik) P25 used as reference photocatalyst. A broad characterisation of the samples allowed us to estimate the percentages of different facets and the amount and form in which the fluorine is found on the surfaces. Good photocatalytic behavior can be ascribed to both high {001} facet exposure and adsorbed fluorine on the photocatalysts surfaces.

Keywords: {001} facet, fluorination, F-TiO2, phenol, Methyl Orange, Cr(VI)

Address correspondence to E-mail: carmen.hidalgo@csic.es

Phone: +34 954489500

1. Introduction

Titanium dioxide (TiO_2) heterogeneous photocatalysis has been widely studied for many environmental applications in water and air pollution control [1-3]. However, even though TiO_2 has many good features as photocatalyst, such as chemical and photochemical stability, non-toxicity and appropriate band positions; it has a major draw-back that is its high recombination rate of photogenerated electron-hole pairs, which reduces considerably the photoefficiency of this oxide in photocatalytic processes [3].

In this context, the development of TiO_2 crystals with specific facets, in order to obtain surfaces with higher reactivity, has been recently studied as a method for improving its efficiency [4-10]. Thus, it has been suggested that the {001} facets of anatase TiO_2 have higher reactivity compared to the more common {101} facets, due to their higher concentration of unsaturated five-coordinated Ti (Ti_{5c}) and high surface energy. It is accepted than surfaces with a higher percentage of undercoordinated atoms are usually more reactive in heterogeneous reactions [11]. Besides, it is known that adsorption properties on a surface depend strongly on surface atomic structures (atomic coordination and arrangements); and different exposition of facets in the TiO_2 photocatalyst would lead to different ability in adsorption of the substrates to be photodegraded. This undoubtedly would have also an influence on the final efficiency of the oxide, where the surface undercoordinated Ti atoms found in {001} facets would display higher reactivity for the dissociative adsorption of reactants; such as water or organic molecules in the reaction media [7,11]. Some studies have also pointed out about the different roles of the different facets. Thus, it has been reported that high-energy {001} facets would provide the oxidative sites and low-energy {101} facets the reductive ones [12,13]. Therefore, even if a high percentage of in {001} facet exposition is desirable; a certain amount of other facets to

obtain an equilibrium in the redox processes is needed. In this sense, to quantify the percentage of exposition of {001} facets seems to be important to understand the activity behaviour of TiO_2.

In this context, many studies have been dedicated to produce TiO_2 where the surface exposition of {001} facet is high. Thus, faceted TiO_2 has been prepared by different methods: sol-gel, hidrothermal, solvothermal, topotactic transformation, epitaxial growth, etc [5]. It is normally required the addition of a capping agent, where a selective adsorption can control growth rates along different orientations [14]. Several compounds have been used and reported to drive to preferential growths of different TiO_2 facets; such as diethanolamine [12-13], carboxylate groups [14], oleic acid or oleylamine [15]. Very often this morphological controlling agent is fluorine, due to its ability to stabilise the preferential growth of reactive {001} facets of anatase TiO_2 [16].

On the other hand, addition of fluorine to TiO_2 surfaces has been used by itself as a method for improving the photocatalytic activity of the oxide. Thus, surface fluorination (ΞTi-F groups) has been reported to reduce the recombination of photogenerated electron-holes by acting as electron-withdrawing centres [17-20]. At the same time, it has also been found that surface fluorination improves the generation of mobile (unbound) OH· radicals that are known to be stronger oxidants that the surface adsorbed OH· radicals [19].

When preparations of faceted TiO_2 using fluorine as capping agent have been reported, often the presence of residual fluorine on the TiO_2 surface is not considered, focusing the studies only in the presence of reactive facets. However, as it has been mention before the presence of ΞTi-F groups can have an important influence in the photocatalytic behaviour of the TiO_2. This has to be borne in mind in those preparations which often do not have a

calcination process at high temperature to assure a clean fluorine-free surface that in those cases would also lead to an important loss of surface area [21].

In the present work, different TiO_2 have been prepared by following a feasible and high yield preparation method using fluorine as capping agent with the aim of tailoring crystal facets of TiO_2. The presence of fluorine on the surface of the final materials has also been considered and studied. As a result, TiO_2 showing high photocatalytic activities for several substrates were obtained, in both photoxidation and photoreduction processes. The good performances were explained in base not only of facet composition but also on the fluorinated surfaces of the oxides. Aware of the importance of quantifying percentages of exposed facets, the study includes two different methods of calculation, based on two very different experimental techniques (RAMAN and TEM). Besides, efficiency of the materials is discussed for both oxidation and reduction processes as a whole, to be able to obtain an overall idea of the photocatlytic behaviour of this faceted TiO_2. Those fluorinated TiO_2 with high {001} facet exposition samples highly exceeded the photocatalytic performance of commercial TiO_2 Degussa (Evonik) P25 used as reference photocatalyst.

2. Material and Methods

2.1 Synthesis procedure

Materials were prepared by direct hydrothermal treatment of the titanium precursors, i.e. Titanium tetraisopropoxide (Aldrich, 97%) or Titanium Butoxide (Aldrich, 97%) with addition of a small amount of acid (HCl or HF), in a volume ratio Ti precursor/acid of 25:4 v/v. The solutions were transferred into a Teflon recipient inside of a stainless steel autoclave and hydrothermal treatment was performed at 200ºC for 24 hours. A precipitate

was obtained and was then filtered, repeatedly washed with distilled water and dried overnight at 100ºC.

Thus, four different samples were obtained depending on the titanium precursor and acid used, and samples were named ButHF, ButHCl, IsoHF and IsoHCl.

Commercial TiO2 Degussa (Evonik) P25 used as reference material was used as received.

2.2 Characterisation techniques

Crystalline phase composition and degree of crystallinity of the samples were estimated by X-ray diffraction (XRD). XRD patterns were obtained on a Siemens D-501 diffractometer with Ni filter and graphite monochromator using Cu Kα radiation.

RAMAN analyses were performed in a LabRAM Horiba Jobin Yvon confocal Raman microscope with three excitation wavelengths (785 cm-1 red, 532 cm-1 green, and 325 cm-1 UV).

BET surface area and porosity measurements were carried out by N_2 adsorption at 77 K using a Micromeritics ASAP 2010 instrument.

Chemical composition and impurities of the samples were determined by X-ray fluorescence spectrometry (XRF) in a Panalytical Axios sequential spectrophotometer. XRF measurements were performed onto pressed pellets (sample included in 10wt% of wax).

Light absorption properties of the samples were studied by UV-Vis spectroscopy. UV-Vis spectra were measured on a Varian spectrometer model Cary 100 equipped with an integrating sphere and using $BaSO_4$ as reference. Band-gaps values were calculated from

the corresponding Kubelka-Munk functions, $F(R\infty)$, which are proportional to the absorption of radiation, by plotting $(F(R\infty)\cdot h\nu)^2$ against $h\nu$.

Field Emission Scanning Electron Microscopy (FESEM) images were obtained in a Hitachi S-4800 microscope used in secondary electron mode with an acceleration voltage of 2 kV (1-3 nm resolution). Samples were dispersed in ethanol using an ultrasonicator and dropped on a carbon grid without any coating of conductive material.

Transmission Electron Microscopy (TEM) was performed in a Philips CM200 instrument. Selected samples were also studied by FEG high resolution transmission electron microscope (HRTEM) from FEI Company (model TECNAI G2 F30 S-twin) with scanning-transmission capabilities (STEM).The measurements were conducted at 300 kV (0.2 nm point resolution). The microscope is equipped with a high angle annular dark field (HAADF) detector from Fischione Instruments (0.16 nm point resolution), and an INCA X-Max 80 silicon drift detector (SDD) for the energy dispersive X-ray analysis (EDX). The HR micrograph analysis, lattice spacing, First Fourier Transform (FFT) and phase interpretation, were done with the Gatan Digital Micrograph software (Gatan Inc.) and the Java version of the Electron Microscope Software (JEM).

X-ray photoelectron spectroscopy (XPS) study was carried out on a Leybold–Heraeus LHS-10 spectrometer, working with constant pass energy of 50 eV. The spectrometer main chamber, working at a pressure $<2 \times 10^{-9}$ Torr, is equipped with an EA-200 MCD hemispherical electron analyser with a dual X-ray source working with Al Kα ($h\upsilon$ = 1486.6 eV) at 120 W and 30 mA. C 1s signal (284.6 eV) was used as internal energy reference in all the experiments. Samples were outgassed in the pre-chamber of the instrument at 150 ºC up to a pressure $< 2 \times 10^{-8}$ Torr to remove chemisorbed water.

2.3 Photocatalytic activity tests

The evaluation of the photocatalytic activity of the samples was performed by mean of three model reactions; the photo-oxidation of phenol (aromatic compound) and Methyl Orange (MO, dye) and the photo-reduction of Potassium Dichromate ($K_2Cr_2O_7$).

Suspensions of the catalysts (1 g/L) in the substrate solution (50 ppm for phenol, 20 ppm for MO and 100 ppm for $K_2Cr_2O_7$) were placed in a 400 ml pyrex discontinuous batch reactor enveloped by an aluminium foil and illuminated through a UV-transparent Plexiglas® top window (threshold absorption at 250 nm) by an Osram Ultra-Vitalux lamp (300 W) with sun-like radiation spectrum and a main line in the UVA range at 365 nm. The intensity of the incident UVA light on the solution was determined with a PMA 2200 UVA photometer (Solar Light Co.), being 80 W/m^2.

Magnetic stirring and a constant oxygen flow were used to produce a homogeneous suspension of the catalyst in the solution. Prior illumination, catalyst-substrate equilibration was ensured by stirring the suspension 30 minutes in the dark. Photocatalytic tests were run for 2 h and samples at different irradiation times were collected and filtered with sterile syringe 0.45 µm pore filters. Then, Phenol concentration was followed by HPLC technique (Agilent Technologies 1200) equipped with UV-Vis detector using an Elipse XDB-C18 column (5 µm, 4.6 x 150mm). Mobile phase was water/methanol (65:35) at a flow rate of 0.8 ml/min. MO and Cr(VI) concentrations were followed by UV-Vis spectroscopy by measuring the intensities of 465 nm and 350 nm bands respectively.

Total mineralisation of phenol and Methyl Orange with the illumination time was followed by measuring the total organic content (TOC) in a Shimadzu 5000 TOC analyser.

Blank experiments were performed in the dark as well as with illumination and no catalyst, without observable change in the initial concentration of phenol, MO and Cr(VI) in all cases.

3. Results and Discussion

XRD pattern of the different samples are depicted in Fig. 1. As it can be seen, ButHF, ButHCl and IsoHF present anatase as only crystalline phase; however, relative intensity of the different peaks varies depending on the sample. On the contrary, the only crystalline phase in sample IsoHCl is rutile.

Anatase TiO_2 generally presents a tetragonal bi-pyramidal structure comprised by the thermodynamically stable {101} facets, and then a much lower percentage of the energetically unfavorable {001} facet [5]. However, (001) surface is considered to be more reactive than (101) surface, due to its high density of surface undercoordinated Ti atoms. Thus, when TiO_2 materials are obtained with a high percentage of exposed {001} facets, a higher photocatalytic activity is expected [4].

The different intensities of the XRD peaks for the samples prepared with HF addition compared to the sample prepared with HCl, give account of a different preferential growth of the TiO_2 crystals in the presence of Fluorine [15,22]. Relative peak intensity ratios for the different crystallographic planes are shown in Table 1. As it can be seen, for the samples prepared with HF, relative intensity of the peaks corresponding to planes 004 decreases while relative intensity for 200 increases for these samples, being this fact more pronounced in sample IsoHF. Here, it can be inferred the role of Fluorine as capping agent in the structure of the obtained TiO_2. Thus, as it will be confirmed later with other techniques,

materials prepared with HF are obtained in different crystal shape, exposing the facet {001} in a higher degree than conventional anatase TiO_2.

On the other hand, the sample prepared with titanium isopropoxide and HCl (IsoHCl) has totally rutilised. Thus, it can be clearly seen the strong influence of the acid used during the synthesis in the final structure of the material.

Raman spectra for ButHF, ButHCl and IsoHF (the samples with anatase as only crystalline phase) are shown in Figure 2. The peaks appearing at 144, 394, 514 and 636 cm-1 for all these samples are indicative of anatase phase, in agreement with XRD studies [23]. However, as it can be seen, relative intensities for the Eg peaks of the samples prepared with HF are lower than the ones for the sample prepared with HCl. At the same time, intensity of A1g peaks increases for the samples prepared with HF. Some authors have used Raman spectroscopy as an approach for measuring the percentage of exposed {001} facets in anatase TiO_2, as the intensity of the A1g and B1g peaks in the Raman spectra of samples with high percentage of {001} facets becomes increased. The percentage of exposed {001} facets is then estimated by the ratio of Raman vibrational modes between Eg and A1g [10, 24]. For ButHF, ButHCl and IsoHF the intensity ratios are depicted in Table 2. The estimated percentages of exposed {001} facet for the samples prepared with HF are 69 and 55% for ButHF and IsoHF respectively. In contrast, percentage for ButHCl, anatase sample prepared with HCl, is only 12%.

BET surface area values for the different samples can be found in Table 1. Samples which consist in anatase phase have relatively high values of surface areas, ranging from 90 to 110 m^2/g. On the contrary, IsoHCl which is rutile possess a much lower value of 12 m^2/g.

Fig. 3 shows pore diameter distribution for the different samples. It can be seen that the range of pore size is larger for the samples prepared with the addition of HF. Thus, ButHF

and IsoHF present a similar pore size distribution with pore diameters between 2 and 100 nm. In contrast, the sample prepared with HCl, ButHCl, presents a narrower range for pore size diameter from 2 to just 20 nm, without larger pores. IsoHCl, rutile sample, presents a very low value of pore volume in the whole range of pore diameters, in concordance with its low surface area value.

UV-Vis light absorption spectra of all the samples were recorded (results not shown for the sake of brevity). The typical sharp absorption band edge of the TiO_2 semiconductor was observed at around of 400 nm for all the samples. From the UV-vis DRS spectra, band gaps energies were calculated, being 3.1-3.2 eV for anatase samples and 2.9 eV for IsoHCl sample. As expected, band gap energy is slightly lower for the rutile material [25]. All values are shown in Table 1.

Representative SEM pictures for the samples are shown in Fig. 4. ButHCl presents particles very heterogeneous in shape and size, as well as high degree of sinterisation. IsoHCl is composed by larger and better defined particles; however, they also present a high heterogeneity in shapes and sizes. On the contrary, samples prepared with HF addition, IsoHF and ButHF, present a similar morphology, composed by square and rectangular platelets with dimensions ranging from around 30 to 80 nm.

ButHF and IsoHF samples were microcharacterised with the TEM miscroscope and selected representative pictures are shown in Fig 5. Both samples are formed by agglomerated nanoparticles in the shape of nanoplatelets ranging in size from 20 to 50 nm, with some larger particles up to 70-80 nm, in agreement with SEM observations. Other elongated nanoparticles can also be observed; nevertheless, after tilting the sample area, the elongated nanoparticles change and transform in platelets, which means that all the particles are platelets deposited either flat or on their side. This would agree with the

contrast of the displayed images in Fig. 5, where a different contrast is observed between platelets and elongated particles. The contrast in a TEM image is directly proportional to the thickness of the particle, since the image is a bi-dimensional projection along the observation axis; platelets are clearer because their thicknesses are very low (about 5 nm, the short measure of the elongated particle); however, the contrast of the elongated particles is darker, its thickness corresponds to the side of the platelet square (approx. 30-50 nm). These results are in good agreement with those observed by SEM (Fig. 4).

HRTEM micrographs of the IsoHF sample oriented along two different zone axes of the tetragonal structure TiO_2-anatase are presented in Figure 6. The planar spacing (Fig. 6b) and a lot of stacking faults and point defects (Fig. 6a) are marked in the images. The [1 1 1] zone axis shows the flat square platelets projection (Fig. 6a-b), the first Fourier transform (FFT) is depicted in the inset of Figure 6b with the corresponding (h k l) planes marked in the FFT. Figure 6c shows a projection of a set of four side platelets, nearly oriented along [1 0 0], from this micrograph it can be clearly seen that the third dimension of the platelets is approx. 5 nm. The corresponding FFT of each side platelet are also inset in the image.

From these TEM studies, measuring a large number of platelets from different zones, the average size dimensions of the platelets could be estimated. Thus, average length of the platelets in IsoHF was 42 nm, while in ButHF was 35 nm. Average platelet width for both samples was 5 nm. According to Fang and col. [26], percentage of exposed {001} facet can be calculated by equation 1, based in geometric and trigonometric estimations, where *l* and *h* are the average width and length of the particles, respectively; and 68.3º is the angle between (001) and (101) planes.

$$\frac{S_{001}}{S_{total}} = \frac{\left(l-\frac{h}{tg68.3}\right)^2}{\left[\left(l-\frac{h}{tg68.3^{\circ}}\right)^2+h\frac{\left(4l-\frac{2h}{tg68,3^{\circ}}\right)}{sen68.3^{\circ}}\right]} \qquad \text{Eq. 1}$$

Applying Eq. 1 to our samples ButHF and IsoHF, percentages of 79% and 76% of {001} facet are obtained respectively (Table 2). These values are higher than those obtained by RAMAN estimations for the same samples, in agreement with reference [24] where it is proven that values obtained by Raman calculations are always a little underestimated. Nevertheless, it was confirmed that samples with a large exposition of {001} facet were obtained and the percentage of this facet was higher for ButHF than for IsoHF sample.

Chemical composition of the samples was studied by XRF. This technique is useful to know the nature and amount of impurities in the samples. In our case, no residual chlorine was found for samples prepared by HCl addition, while fluorine could be found in ButHF and IsoHF samples, in an amount of 5.1 and 3.6 % respectively.

As the amount of fluorine in the samples is relatively notable, XPS measurements were performed to study whether this element was on the surface and in which chemical form. Fig. 7 shows XPS F 1s region spectra for the samples. In both samples, a well-defined single peak at binding energy of 683.9 eV can be seen, ascribed to fluoride in Ti-F on the TiO_2 surface, which can be formed by ligand exchange reaction between F^- ions and the surface hydroxyl groups on the TiO_2 surface [27]. In the same way, subtitutional F in solid solution $TiO_{2-x}F_x$ (binding energy at 688.9 eV) can be discarded in these samples.

The presence of Fluorine itself adsorbed on the samples can have a strong influence on the photocatalytic properties of the TiO_2, as it has been reported in several studies [17,28]. Surface Ti-F groups have a strong electron-withdrawing ability and are capable of increasing lifetime of the photogenerated charges; thus, electron-hole recombination rate

can be decreased. Besides, it has also been studied that surface fluorination of TiO_2 can promote the generation of mobile (unbound) OH· radicals, which are more efficient oxidants that surface adsorbed ones [29]. In this context, fluorination of TiO_2 has been used as a strategy to increase its photocatalytic efficiency.

Thus, it seems important to keep in mind the probable presence of residual Fluorine species coming from the capping agents used during the synthesis of faceted TiO_2 when the improvement of the photocatalytic activity of these materials is discussed. The presence of residual surface Fluorine is not checked in many of these studies; and however, its contribution to the improvement of the photocatalytic efficiency cannot be discarded.

Fig. 8 and 9 show degradation profiles of phenol and Methyl Orange over the different samples. Degradation profiles over TiO_2 Degussa P25 have been added as reference. As insets in the figures, linear fitting graphs are shown for both substrates. From these graphs, apparent rate constants were estimated and the corresponding values are shown in Table 3. For both substrates the tendency is the same; i.e. from more to less efficiency IsoHF>ButHF>P25>>ButHCl>IsoHCl. As it can be seen, degradation is faster over samples prepared with the addition of HF, for both substrates phenol and MO, faster also than over P25 the commercial photocatalyst used as reference. The fact that the sample with the highest percentage of exposed {001} facet; i.e. ButHF, presents less activity for the two evaluated substrates indicates that there is also a limit in the facet exposition above which a higher exposure has not longer a positive effect for the activity. This could be related to the spatial separation of redox sites in the different facets, oxidation sites in {001} facets and reduction sites in {101} facets, as it has been reported [12-13, 30], with the necessity of finding an optimal ratio between both facets to optimise the redox processes.

Total Organic Carbon (TOC) values at the end of the reactions give account of the degree of mineralisation of the processes. Thus, after the 2 h test for phenol degradation with the photocatalyst P25, TOC goes from a value of 38 ppm to 3 ppm, which indicates a good degree of total mineralisation of phenol. With IsoHF and ButHF, TOC values decrease bellow 2 ppm for both samples after the 2 h illumination tests for phenol degradation. Thus, not only the reaction rates for IsoHF and ButHF samples are faster than for P25, but also their degrees of total mineralisation are also higher. Same situation can be found in MO tests. These results confirm that no resistant intermediates are formed and that phenol and MO are totally degraded to CO_2.

As some studies reported that the enhancement of photoactivity of faceted TiO_2 is due to an improved oxidation step, where {001} facets provides effective oxidation sites [5,7,30]; we wanted to evaluate these materials also in a reduction process, i.e. the photoreduction of Cr(VI) to less harmful Cr(III). Fig. 10 shows reduction profiles over the different samples, without and with sacrificial agent in Fig.10 (up) and Fig.10 (down), respectively. Corresponding linear fitting graphs are shown as insets in both figures. Apparent rate constants are depicted in Table 3. The addition of 2-propanol (0.2 M) as sacrificial agent provided an organic substance to act as electron donor in the media capturing the photogenerated holes. When no sacrificial agent is used, the activity for the samples prepared with HF is similar to the activity of the reference P25. Thus, in our case, faceted materials do not have a detrimental effect in a reduction process (if compared with P25 behaviour). In this process, fluorination probably compensates the decrease of reduction sites of faceted surfaces. Fluorinated TiO_2 surfaces enhance the OH groups formation which favour Cr(VI) adsorption and therefore could help its photoreduction. When a sacrificial agent is added to the reaction media, the reduction of Cr(VI) is faster over all the

samples; specially over the samples prepared with HF. As a result of the addition of the sacrificial agent, holes generated on TiO_2 are consumed, supressing electron-hole recombination, and more electrons are available to contribute to reductive processes [31].

In order to better visualise the photocatalytic performance of the different samples, initial reaction rates for the three substrates over all the samples are depicted in Fig. 11. It can be clearly seen the positive effect of the addition of HF during the synthesis; being IsoHF the sample with the better photocatalytic behaviour for the three reaction evaluated. Samples prepared with HF have an increment between 300 and 700% (depending on the substrate) in the reaction rates respect to their HCl counterparts. For the oxidation reactions, reaction rates with the faceted samples also exceed the rates with P25, being approximately the same for the reduction of Cr(VI). These results show that with a simple and high yield preparation method, fluorinated TiO_2 with a high exposition of {001} facet can be obtained with excellent photocatalytic behaviour for both, oxidation and reduction processes.

4. Conclusions

By a simple hydrothermal one-pot synthesis, anatase TiO_2 samples with high {001} facet exposition were obtained. Faceted TiO_2 samples showed an excellent photocatalytic activity for the three substrates evaluated, in both oxidation and reduction reactions. The importance of considering residual fluorine from the addition of the capping agent in the preparation of faceted anatase TiO_2 could be seen. The good photocatalytic performance of these samples can be ascribed to their structural properties of facet composition and to the fluorination effect of residual fluorine on their surfaces.

Acknowledgements

This work was supported by research fund from Project Ref. CTQ2015-64664-C2-2-P (MINECO/FEDER UE). CITIUS (University of Seville) is acknowledged for XRF and XPS measurements.

References

[1] Schneider J, Matsuoka M, Takeuchi M, Zhang J, Horiuchi Y, Anpo M, Bahnemann DW (2014) Understanding TiO2 Photocatalysis: Mechanisms and Materials, Chem Rev 114: 9919-9986.

[2] Chen X, Mao SS (2007) Titanium Dioxide Nanomaterials: Synthesis, Properties, Modifications and Applications, Chem Rev 107:2891-2959.

[3] Chen J, Qiu F, Xu W, Cao S, Zhu H (2015) Recent progress in enhancing photocatalytic efficiency of TiO2-based materials, Appl Catal A 4 95:131- 140.

[4] Fang WQ, Gong X-Q, Yang HG (2011) On the Unusual Properties of Anatase TiO_2 Exposed by Highly Reactive Facets, J Phys Chem Lett 2:725-734.

[5] Grabowska E, Diak M, Marchelek M, Zaleska A (2014) Decahedral TiO_2 with exposed facets: Synthesis, properties, photoactivity and applications, Appl Catal B 156-157:213-235.

[6] Wang Z, Lv K, Wang G, Deng k, Tang D (2010) Study on the shape control and photocatalytic activity of high-energy anatase titania, Appl Catal B 100:378-385.

[7] Liu G, Yang HG, Pan J, Yang YQ, Lu GQ, Cheng H-M (2014) Titanium dioxide crystals with tailored facets, Chem Rev 114:9559-9612.

[8] Luan Y, Jing L, Wu J, Xie M, Feng Y (2014) Long-lived photogenerated charge carriers of 001-facet-exposed TiO2 with enhanced thermal stability as an efficient photocatalyst, Appl Catal B 147:29-34.

[9] Lin W, Zheng H, Zhang P, Xu T (2016) Pt deposited TiO2 films with exposed {001} facets for photocatalytic degradation of a pharmaceutical pollutant, Appl Catal A 521:75-82.

[10] Yang L, Zhang Q, Wang W, Ma S, Zhang M, Lv J, He G, Sun Z (2016) Tuning the photoelectronic and photocatalytic properties of single-crystalline TiO2 nanosheet array films with dominant {001} facets by controlling the hydrochloric acid concentration, J Mater Sci 51:950–957

[11] Gong X-Q, Selloni A (2005) Reactivity of Anatase TiO_2 Nanoparticles: The Role of the Minority (001) Surface, J Phys Chem B 109:19560-19562.

[12] Roy N, Sohn Y, Pradhan D (2013) Synergy of Low-Energy {101} and High-Energy {001} TiO2 Crystal Facets for Enhanced Photocatalysis, ACS Nano 7:2532-2540.

[13] Roy N, Park Y, Sohn Y, Leung KT, Pradhan D (2014) Green Synthesis of Anatase TiO2 Nanocrystals with Diverse Shapes and their Exposed Facets-Dependent Photoredox Activity, ACS Appl. Mater. Interfaces 6: 16498-16507.

[14] Kim EY, Choi H, Whang CM (2010) Controlled growth of TiO2 nanorods capped with carboxylate groups by the solvothermal process, J Mater Sci 45: 3895-3900.

[15] Dinh C-T, Nguyen T-D, Kleitz F, Do T-O (2009) Shape-controlled synthesis of highly crystalline titania nanocrystals, ACS Nano 3:3737-3743.

[16] Dozzi MV, Selli E (2013) Specific facets-dominated anatase TiO2: Fluorine-mediated synthesis and photoactivity, Catalysts 3:455-485.

[17] Murcia JJ, Hidalgo MC, Navío JA, Araña J, Doña-Rodríguez JM (2015) Study of the phenol photocatalytic degradation over TiO2 modified by sulfation, fluorination, and platinum nanoparticles photodeposition, Appl Catal B 179:305-312.

[18] Vohra MS, Kim S, Choi W (2003) Effects of surface fluorination of TiO2 on the photocatalytic degradation of tetramethylammonium, J Photochem Photobiol A 160:55-60.

[19] Liu S, Yu J, Cheng B, Jaroniec M (2012) Fluorinated semiconductor photocatalysts: Tunable synthesis and unique properties, Adv Colloid Interface Sci 173:35-53.

[20] Park H, Choi W (2004) Effects of TiO_2 Surface Fluorination on Photocatalytic Reactions and Photoelectrochemical Behaviors, J Phys Chem B 108:4086–4093.

[21] Yang HG, Liu G, Qiao SZ, Sun CH, Jin YG, Smith SC, Zou J, Cheng HM, Lu GQ (2009) Solvothermal synthesis and photoreactivity of anatase TiO_2 nanosheets with dominant {001} facets, J Am Chem Soc 131:4078–4083.

[22] Ye L, Liu J, Tian L, Peng T, Zan L (2013) The replacement of {101} by {010} facets inhibits the photocatalytic activity of anatase TiO2, Appl. Catal B 134-135:60-65.

[23] Golubovic A, Scepanovic MS, Kremenovic A, Askrabic S, Berec V, Dohcevic-Mitrovic Z, Popovic ZV (2009) Raman study of the variation in anatase structure of TiO_2 nanopowders due to the changes of sol-gel synthesis conditions, J Sol-Gel Sci Technol 49:311–319.

[24] Tian F, Zhang Y, Zhang J, Pan C (2012) Raman spectroscopy: A new approach to measure the percentage of anatase TiO 2 exposed (001) facets, J Phys Chem C 116:7515-7519.

[25] Scanlon DO, Dunnill CW, Buckeridge J. Shevlin SA, Logsdail AJ, Woodley SM, Catlow RA, Powell MJ, Palgrave RG, Parkin IP, Watson GW, Keal TW, Sherwood P, Walsh A, Sokol AA (2013) Band alignment of rutile and anatase TiO_2, Nature Mater 12:798-801.

[26] Fang W, Yang X, Zhu H, Li Z, Zhao H, Yao X, Yang HG (2012) Yolk@shell anatase TiO_2 hierarchical microspheres with exposed {001} facets for high-performance dye sensitized solar cells, J Mater Chem 22:22082-22089.

[27] Yu JC, Yu J, Ho W, Jiang Z, Zhang L (2002) Effects of F^- doping on the photocatalytic activity and microstructures of nanocrystalline TiO_2 powders, Chem Mater 14:3808-3816.

[28] Iervolino G, Vaiano V, Murcia JJ, Rizzo L, Ventre G, Pepe G, Campiglia P, Hidalgo MC, Navío JA, Sannino D (2016) Photocatalytic hydrogen production from degradation of glucose over fluorinated and platinized TiO_2 catalysts, J Catal 339:47-56.

[29] Mrowetz M, Selli E (2005) Enhanced photocatalytic formation of hydroxyl radicals on fluorinated TiO_2, Phys Chem Chem Phys 7:1100–1102.

[30] Ohno T, Sarukawa K, Matsumura M (2002) Crystal faces of rutile and anatase TiO_2 particles and their roles in photocatalytic reactions, New J Chem 26:1167-1170.

[31] Chen G, Feng JI, Wang W, Yin Y, liu H (2017) Photocatalytic removal of hexavalent chromium by newly designed and highly reductive TiO2 nanocrystals, Water Res. 108:383-390.

Figure captions

Figure 1. XRD pattern of the different samples: ButHF (a), ButHCl (b), IsoHF (c) and IsoHCl (d).

Figure 2. Raman spectra for the indicated samples: ButHF, ButHCl and IsoHF.

Figure 3. Pore diameter distribution for the different samples: ButHF, ButHCl, IsoHF and IsoHCl.

Figure 4. Representative SEM pictures of the different samples.

Figure 5. Representative TEM pictures for the fluorinated samples: ButHF (A and B) and IsoHF (C and D).

Figure 6. HRTEM results for ISOHF sample showing a flat nanoplatelet projection oriented along the [111] zone axis of anatase TiO2 (a and b) and four side platelets projection orientated along the [100] zone axis (c). The FFT of each nanocrystal are depicted on the corresponding HR images.

Figure 7. XPS spectra of the F1s region for the indicated samples: ButHF and IsoHF.

Figure 8.Phenol degradation profiles over the different samples. Linear fitting graphs as inset.

Figure 9. Methyl Orange degradation profiles over the different samples. Linear fitting graphs as inset.

Figure 10. Cr(VI) reduction profiles over the different samples, without (up) and with (down) addition of isopropanol as sacrificial agent. Linear fitting graphs as inset.

Figure 11. Initial reaction rates for the different samples in the indicated substrates.

Figure 1

Click here to download Figure Fig1_DRX.docx

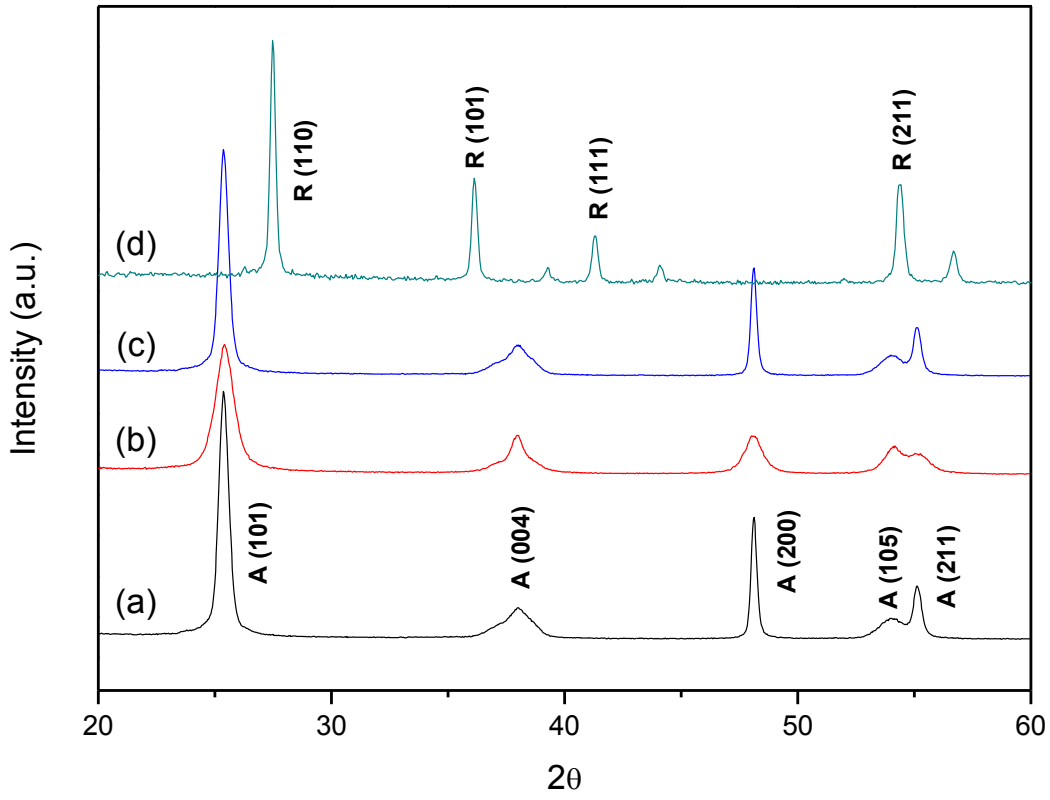

Figure 2

Click here to download Figure Fig2_Raman.docx

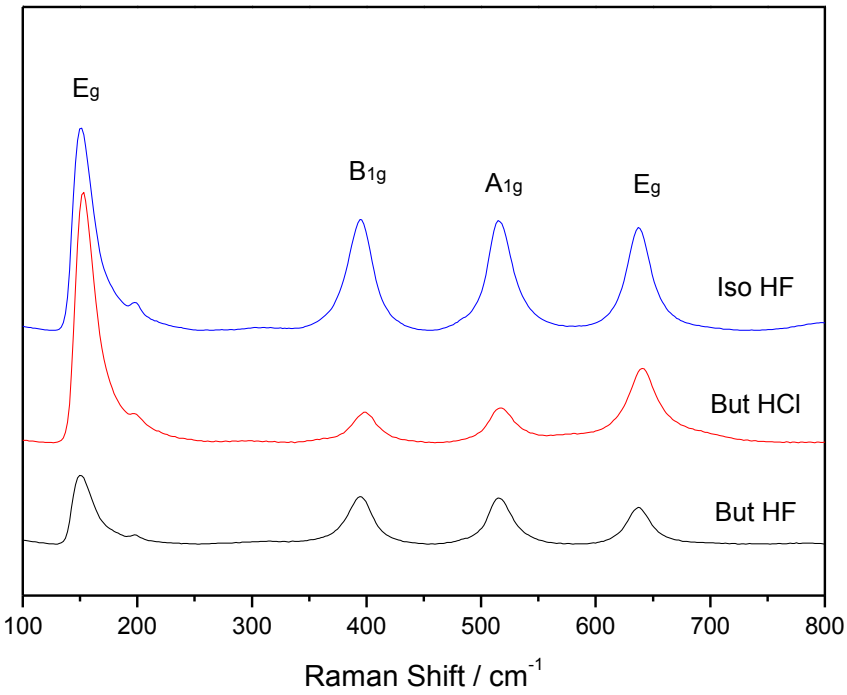

Figure 3

Click here to download Figure Fig3_PoreDiameter.docx

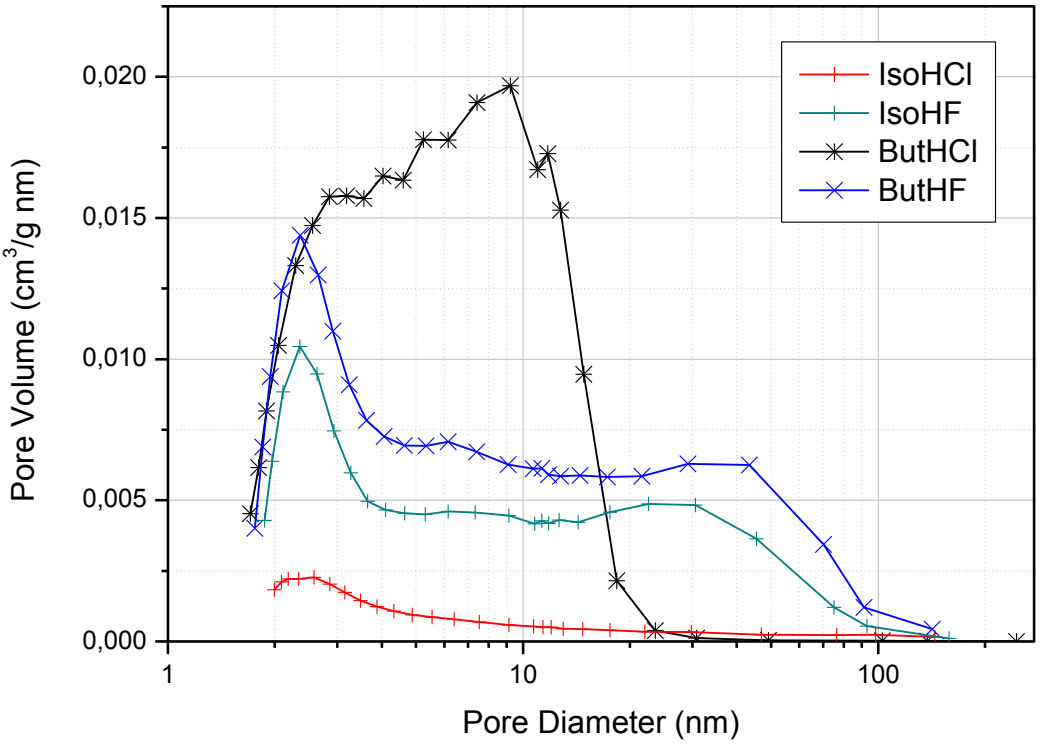

Figure4-MOD

Click here to download Figure Fig4_SEMMOD.docx

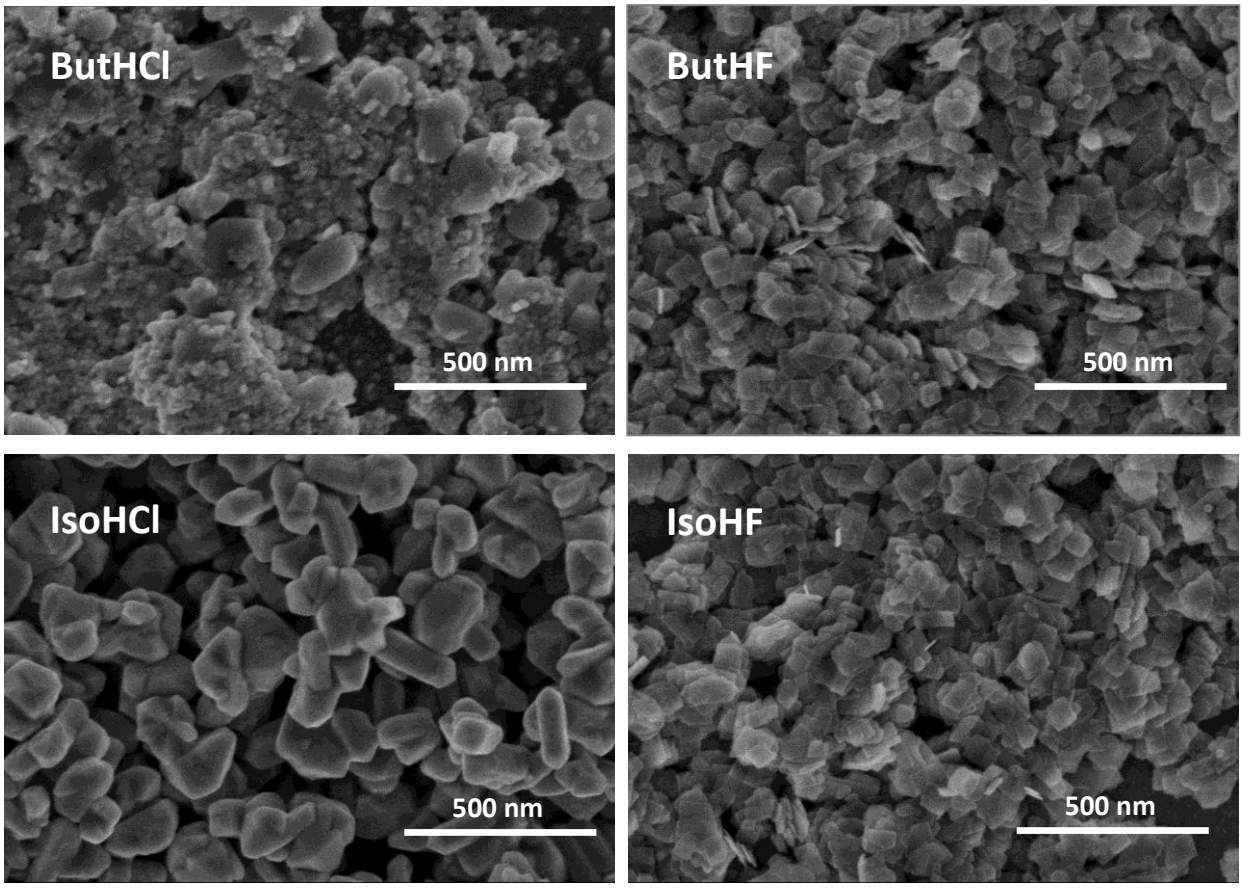

Figure 5

Click here to download Figure Fig5_TEM1.docx

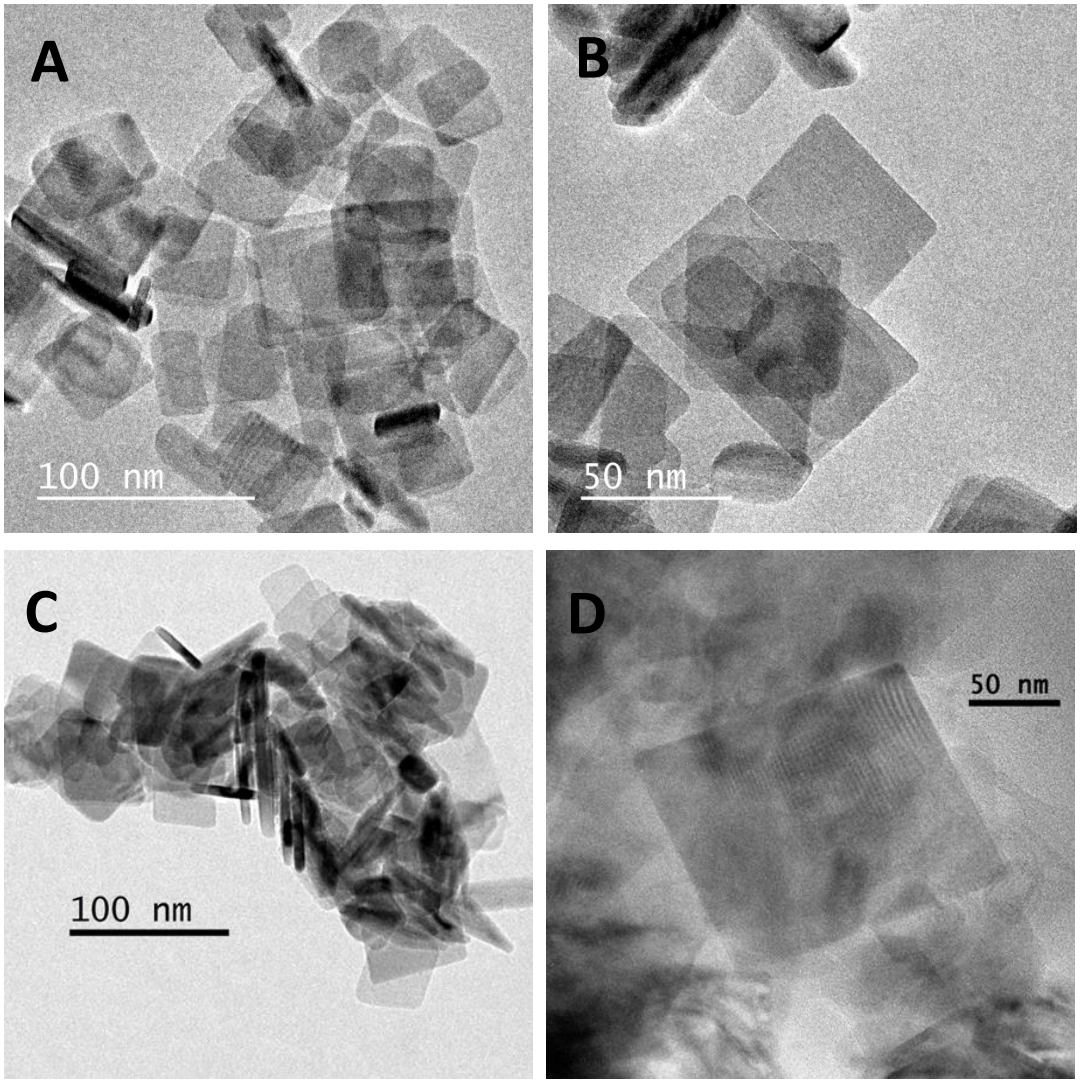

Figure 6

Click here to download Figure Fig6_TEM2.docx

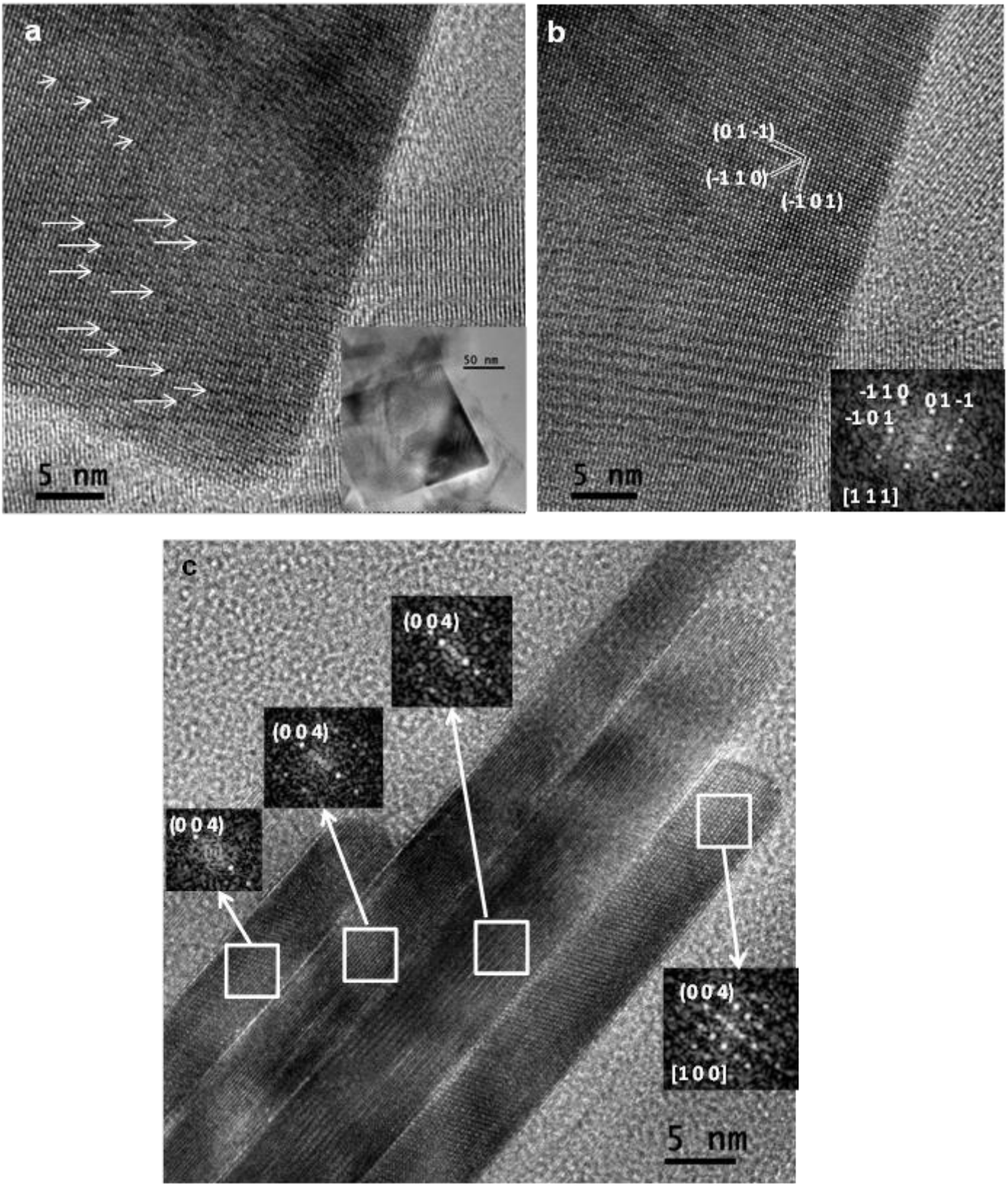

Figure 7

Click here to download Figure Fig7_XPS.docx

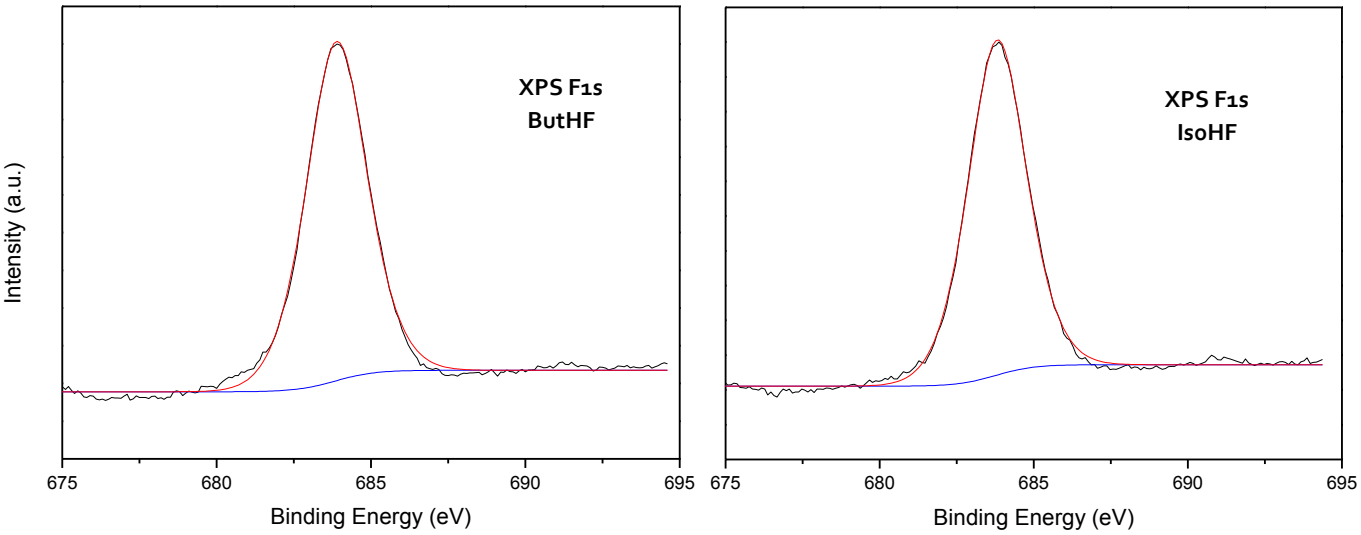

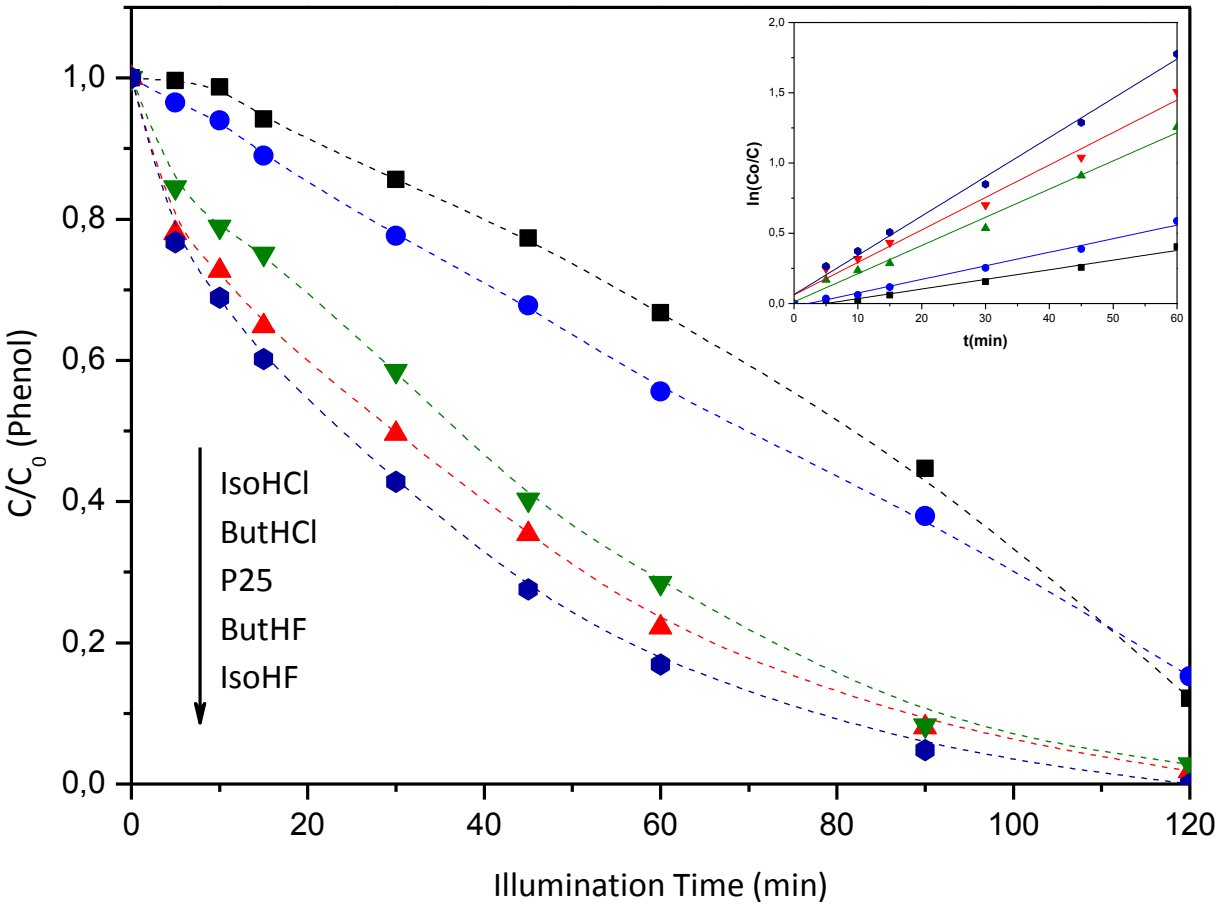

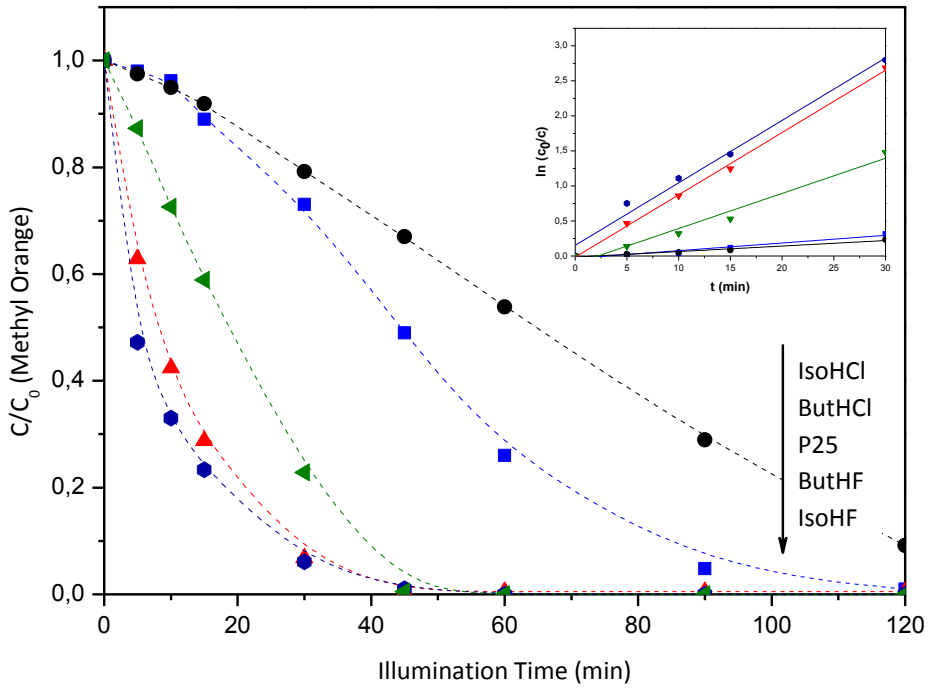

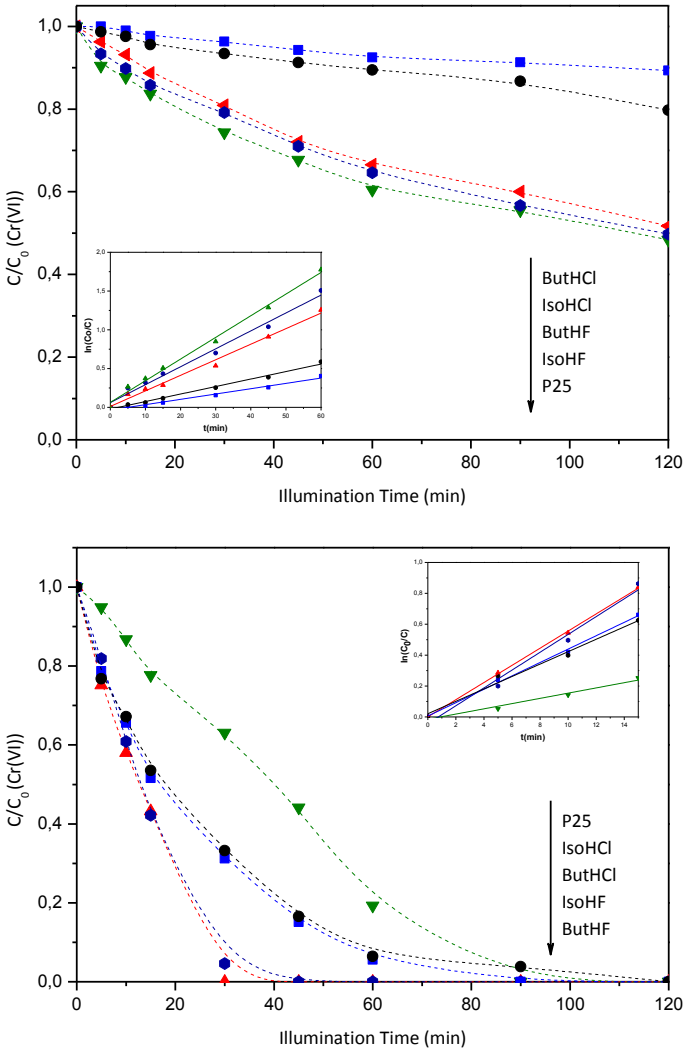

Figure 11

Click here to download Figure Fig11_Vr.docx

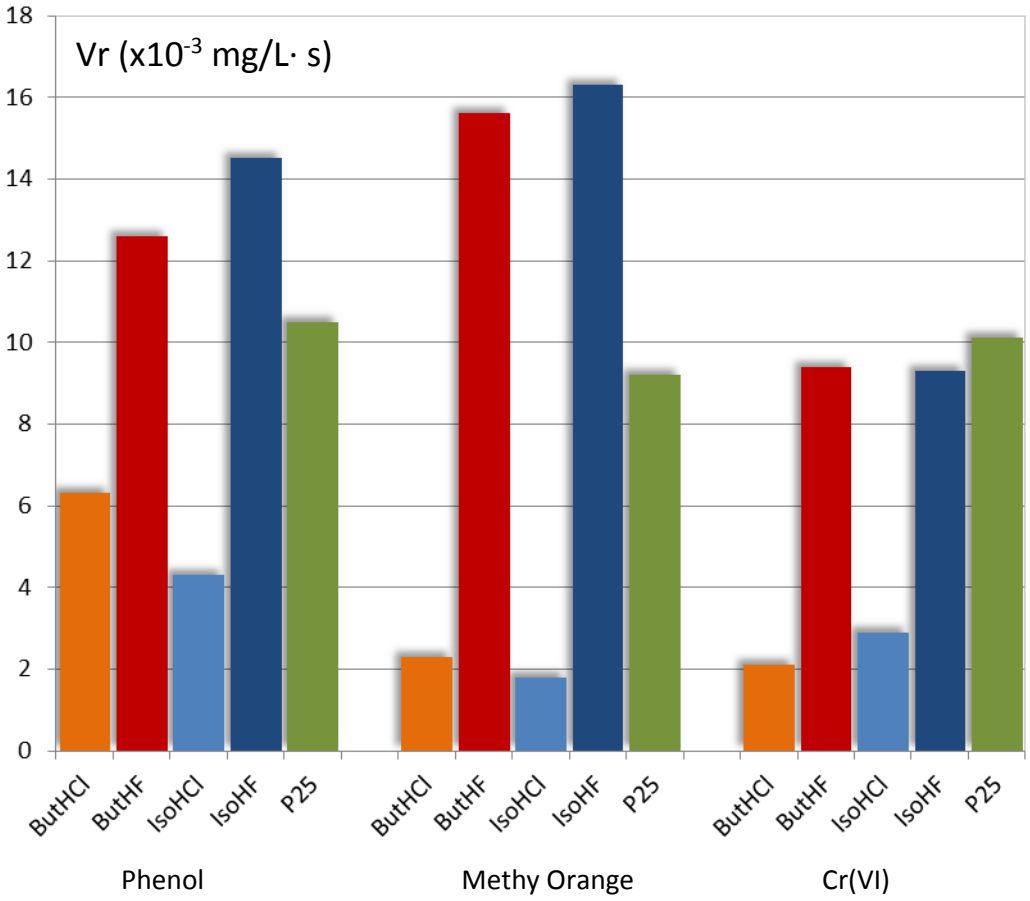

Table 1. Characterisation results

	XRD anatase peaks relative intensities			SBET (m2/g)	Band Gap (eV)
	I(004)/I(101)	I(200)/I(101)	I(211)/I(105)		
ButHF	0.12	0.50	1.80	96	3.1
ButHCl	0.31	0.30	0.96	113	3.2
IsoHF	0.13	0.49	1.10	91	3.1
IsoHCl	-	-	-	12	2.9
P25	-	-	-	50	3.1

Table 2. RAMAN peak intensities and 001 facet percentages

Sample	Peak intensity of Eg	Peak intensity of A1g	Ratio Eg/A1g	[% 001]*	[%001]**
But HF	3745	2510	1.49	69%	79%
But HCl	13655	1853	7.37	12%	-
Iso HF	10995	5956	1.85	55%	76%

*according to Raman as in reference [21] **according to geometric measurements in TEM

Table 1. Apparent rate constants for the different substrates.

	Kk (min^{-1})			
	Phenol	MO	Cr(V)	Cr(VI)+ 2PrOH
ButHF	0,0231	0,0889	0,0068	0,0577
ButHCl	0,0097	0,0109	0,0013	0,0433
IsoHF	0,0279	0,0892	0,0069	0,0555
IsoHCl	0,0069	0,0079	0,0018	0,0402
P25	0,0201	0,0501	0,0078	0,0169